Picosecond acoustic phonon dynamics in $LaF_3:Pr^{3+}$

Sean M. Kirkpatrick,* Ho-Soon Yang, and W. M. Dennis
Department of Physics and Astronomy, University of Georgia, Athens, Georgia 30602
(Received 24 November 1997)

A plasma switching technique is used to generate subnanosecond, far-infrared (FIR) pulses with frequency 113 cm^{-1}. The generation of subnanosecond FIR pulses enables us to improve the time resolution of phonon spectroscopic measurements from 50 ns to 350 ps. As an application of this technique, we investigate the subnanosecond dynamics of high-frequency phonons in 0.5% $LaF_3:Pr^{3+}$. In particular, we report on the generation and detection of a subnanosecond nonequilibrium phonon population at 113 cm^{-1}, and the temporal evolution of the resulting decay products. The frequency dependence of the phonon relaxation rates of acoustic phonons in this material is found to deviate from the ω^5 frequency dependence predicted by an isotropic model with linear dispersion. A more realistic model based on the actual dispersion curves of the material is presented and compared with the data. [S0163-1829(98)08433-1]

I. INTRODUCTION

We have previously demonstrated that a nonequilibrium acoustic-phonon population can be generated in $LaF_3:Pr^{3+}$ (0.5%) by defect-induced one-phonon absorption (DIOPA) of far-infrared radiation[1] (FIR) and that the lifetimes of these phonons can be measured using anti-Stokes absorption vibronic sideband phonon spectroscopy (AVSPS).[2] From this earlier data, we determined that the decay rates of acoustic phonons in the frequency range 22–52 cm^{-1} in $LaF_3:Pr^{3+}$ (0.5%) exhibit a frequency dependence that is in reasonable agreement with an isotropic model with linear dispersion. This model predicts a ω^5 frequency dependence for the decay rate of acoustic phonons by three phonon anharmonic processes.[3,4]

The time resolution of these experiments[1,5] was limited by the pulsewidths of the FIR superadiant source (50 ns) and the tunable dye laser (5 ns), used for phonon generation and detection, respectively. While this time resolution was adequate for studying phonons with frequencies less than $\sim$50 cm^{-1} in $LaF_3:Pr^{3+}$, higher frequency phonons are expected to decay on a subnanosecond time scale. In order to investigate the dynamics of high-frequency phonons farther into the dispersive region of the zone, a plasma switching technique is used to generate 350 ps FIR pulses. These subnanosecond FIR pulses, in conjunction with a short pulse (236 ps) tunable dye laser, enable us to increase the time resolution of the DIOPA and AVSPS techniques, and measure the lifetimes of phonons with frequencies up to 113 cm^{-1}.

Plasma switching of the midinfrared radiation from a CO_2 laser was observed by Alcock *et al.*,[6] this technique was later extended to the femtosecond range (at $\sim$10 μm) by Rolland and Corkum.[7] At longer wavelengths, Salzmann, Vogel, and Dodel[8] reported switching of 119 μm far-infrared radiation using the 2 ns pulses from a N_2 laser to induce photocarriers in both silicon and gallium arsenide.

High-purity silicon which transmits at FIR frequencies, photoconducts when irradiated with light with photon energies higher than the band gap (1.11 eV or $\lambda < 1.2$ μm).[9] When a large number of photocarriers have been excited Si becomes reflecting at long wavelengths. This change in reflectance can be exploited to optically switch FIR radiation. In this work, the switching pulse is the ($\lambda_L = 532$ nm, $\tau_p = 130$ ps) output from a mode-locked frequency doubled YAG:Nd^{3+} laser. The FIR pulse can be switched by ensuring the optical pulse is synchronized with the center of the FIR pulse at the Si wafer. In this case the first half of the FIR pulse is transmitted while the second half is reflected. Performing this operation twice, once in reflection and once in transmission, allows a significantly shorter FIR pulse to be sliced out of the original 50 ns FIR pulse.

The width of the sliced FIR pulse is determined by the optical path difference between the two lasers at the semiconducting wafers and is ultimately limited by the pulse width of the switching laser. In this paper, we report pulse slicing of far-infrared radiation at 113 cm^{-1} (88 μm) and the generation of 350 ps pulses at this frequency. Since the free-carrier excitation in silicon occurs on a subpicosecond time scale, the rise and fall times of the switched pulse are limited by the risetime of the 532 nm laser pulse.

We use the ultrashort FIR pulses generated by the above technique to investigate the dynamics of high-frequency phonons in $LaF_3:Pr^{3+}$. We compare our results with both the standard isotropic model with linear dispersion and a more realistic model which takes into account some of the details of the dispersion curves in this material.

II. EXPERIMENT

A. Generation of subnanosecond FIR radiation

FIR pulses with frequency 113 cm^{-1}, a pulse energy of 16 mJ and a nominal pulse width of 50 ns were generated using a CH_3F superradiant cell pumped by a transverse excited atmospheric pressure CO_2 laser.[10] Picosecond FIR pulses are generated by plasma switching the nanosecond pulse using two (1 mm thick) silicon wafers.

In order to determine the minimum energy flux required to switch the FIR transmission of the silicon wafer, intensity-dependent transmission measurements were performed (see Fig. 1). For these measurements, the Si wafer was oriented

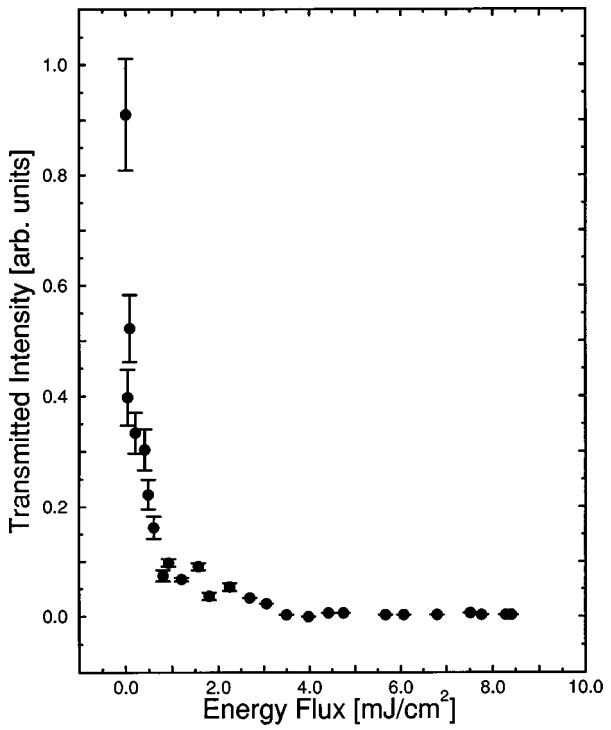

FIG. 1. Transmission of FIR radiation at 113 cm^{-1} through a 1 mm thick silicon wafer as a function of the incident 532 nm energy flux.

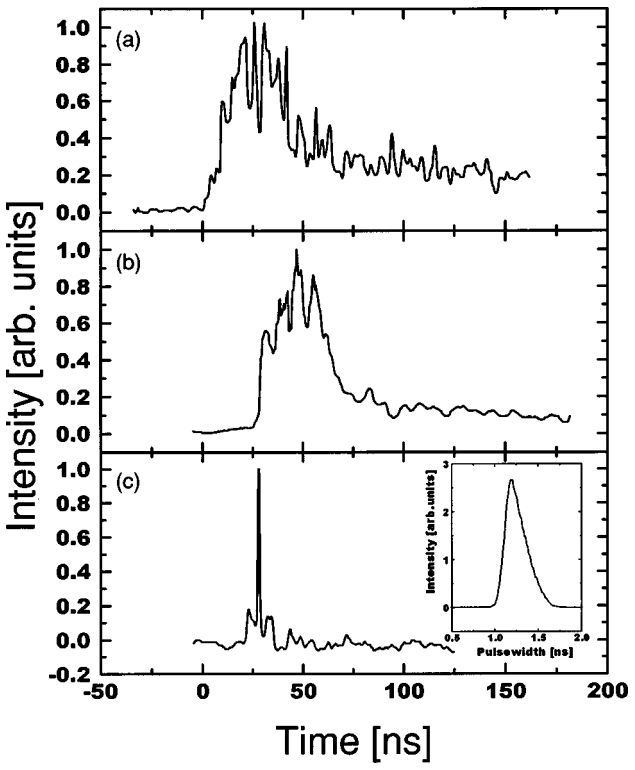

FIG. 2. Far-infrared pulse profile: (a) prior to switching, (b) after switching once, and (c) after switching twice. The inset shows the short cavity dye laser pulse profile as measured by time correlated photon counting. Values for the FIR and optical pulse widths are 350 and 236 ps, respectively.

such that the polarization of the FIR pulse was perpendicular to the plane of incidence, and a pyroelectric energy meter was positioned directly behind the wafer. The transmitted FIR energy was then measured as a function of the energy flux of the frequency doubled (532 nm) YAG:Nd^{3+} pulse. In the absence of an incident 532 nm pulse, each wafer was found to transmit $90\% \pm 5\%$ of the incident FIR radiation at Brewster's angle. For an incident energy flux greater than 4 mJ/cm^2 the transmitted far infrared radiation was found to go to zero to within our experimental accuracy. Each wafer was found to reflect $75\% \pm 4\%$ of the FIR pulse energy at a 532 nm energy flux of 11 mJ/cm^2. This was the nominal energy flux used in our experiment.

The intrinsic carrier density, at room temperature, of silicon[11] is $\sim 10^{10}$ carriers/cm^3. For the case of a 1 cm^2 spot size and 50% absorption of the incident (11 mJ/cm^2) energy flux at 532 nm, we estimate the photoinduced free-carrier concentration in the activation region to be $\sim 10^{18}$ carriers/cm^3. Based upon the above carrier concentration and the recombination rate of high-purity silicon calculated by Shur,[12] we estimate the carrier lifetime to be $\sim$10 ms. This is in reasonable agreement with the carrier lifetime of 5 ms measured by Tyagi *et al.*[13] for a carrier concentration of $\sim 10^{18}$ carriers/cm^3. Since the FIR pulsewidth is several orders of magnitude shorter than the carrier lifetime, variations of the reflectivity due to carrier recombination can be ignored.

The experimental setup used to optically switch FIR radiation is as follows: An off-axis parabolic mirror (OAP) is used to focus the (50 ns) FIR pulse onto the first silicon wafer at Brewster's angle. The optical pulses (used for plasma switching) are generated by a Continuum YG671C active-passive mode locked, internally *Q*-switched, frequency doubled YAG:Nd^{3+} laser. The internal *Q* switch provides low pulse to pulse jitter at the expense of increasing the pulse width to 130 ps. The fundamental 1.06 μm YAG:Nd^{3+} pulse width was measured to be 130 ps using an autocorrelator. The frequency doubled (532 nm) pulse is electronically synchronized with the center of the 50 ns FIR pulse at the first silicon wafer using a Stanford Research DG535 digital delay pulse generator. The fast risetime of the optical pulse effectively slices the FIR pulse in half causing a sharp leading edge to be observed in reflection. The reflected portion of the FIR pulse is recollimated and then focused onto the second silicon wafer by means of two OAP mirrors. The reflected 532 nm pulse from the first wafer is directed onto the second wafer with a delay of 350 ps with respect to the reflected FIR pulse. Finally, the resulting transmitted FIR pulse is recollimated with an OAP.

Using a Tektronix C1001 digitizing scope camera, a Molectron P5-01 pyroelectric detector, and a Tektronix 2467B, 400 MHz oscilloscope, digital images of the FIR pulse were taken before switching [Fig. 2(a)], after switching once [Fig. 2(b)], and after switching twice [Fig. 2(c)].

We note that the electronic jitter between the 130 ps optical pulse and the 50 ns FIR pulse is ± 20 ns and is thus within the pulsewidth of the FIR. After plasma switching the subnanosecond FIR pulse is locked to the optical pulse and the electronic timing jitter is transformed into an amplitude instability of the switched FIR pulse.

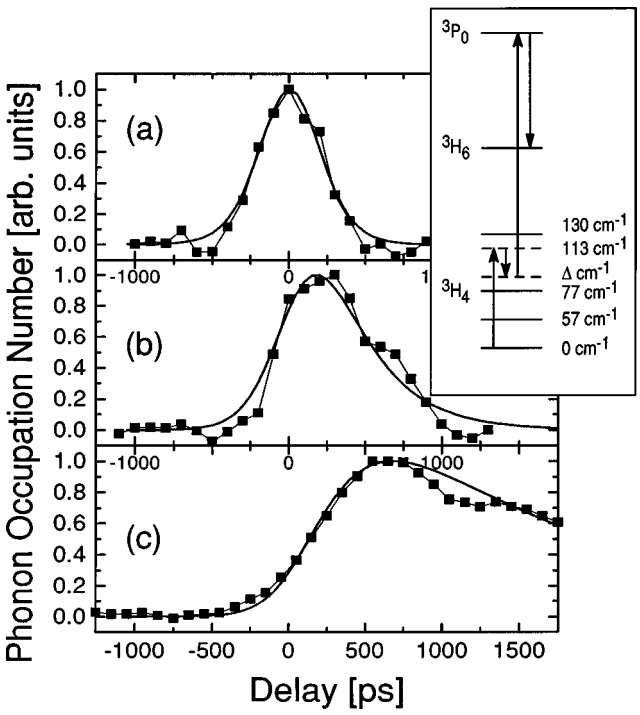

FIG. 3. Nonequilibrium phonon transients for phonons of frequency: (a) 113 cm^{-1}, (b) 75 cm^{-1}, and (c) 55 cm^{-1}. The inset shows the energy-level diagram for Pr^{3+} illustrating phonon detection by anti-Stokes absorption vibronic sideband phonon spectroscopy.

B. Picosecond phonon dynamics

In this section we describe the use of ultrashort FIR pulses to investigate the dynamics of high-frequency phonons in LaF_3:Pr^{3+}.

A schematic of the energy levels of Pr^{3+} which are relevant to this experiment is shown in the inset to Fig. 3. In particular, nonequilibrium phonons with frequency 113 cm^{-1} are generated by defect-induced one-phonon absorption of FIR radiation and time-resolved frequency selective phonon detection is achieved using absorption vibronic sideband phonon spectroscopy. Since the experimental setup for the nanosecond versions of these techniques have been described in detail elsewhere,[5,14] only those details pertaining to extending these techniques to the picosecond time regime will be described in this paper.

Phonon generation is implemented using the 350 ps FIR pulses generated by the plasma switch described in the previous section. Initially, a nonequilibrium phonon population at 113 cm^{-1} is generated. This nonequilibrium population is expected to subsequently decay into a broadband distribution at lower frequencies. An examination of the fluorescence spectrum of LaF_3:Pr^{3+} indicates that the FIR pulse with frequency 113 cm^{-1}, in addition to pumping the defect-induced one-phonon absorption band, may also pump the wing of the 130 cm^{-1} crystal-field split level of the ground-state manifold. That is, in addition to phonon generation by DIOPA, phonons may also be generated by nonradiative decay within the ground-state manifold.

Phonon detection is implemented by detuning a picosecond dye laser an amount Δ from the $^3H_4 \rightarrow {}^3P_0$ transition of Pr^{3+}. In this case absorption of the dye laser pulse only occurs if there is a nonequilibrium phonon population at frequency Δ. The absorption of the dye laser pulse is detected by monitoring the fluorescence from the $^3P_0 \rightarrow {}^3H_6$ transition. Phonon transients are measured by delaying the optical (detection) pulse with respect to the FIR (generation) pulse.

The optical pulses used for phonon detection by AVSPS are generated by pumping a short cavity (1.5 cm) Coumarin 480 dye laser, configured in Littrow, with the frequency tripled (355 nm) output of the YAG:Nd^{3+} laser. This dye laser produces a 236 ps pulse with a nominal pulse energy of 10 μJ. The broad background due to amplified spontaneous emission is removed by an external spectrometer and an angle-tuned interference filter. The dye laser pulse width was measured to be 236 ps (see inset to Fig. 2) using an Hamamatsu PLP-01 multichannel plate photomultiplier tube and time-correlated photon counting electronics.

The FIR pulse is focused into the sample using an OAP mirror, while the optical pulse is focused into the sample in a direction counterpropagating to the FIR pulse. An adjustable temporal delay between the optical pulse and the FIR pulse is implemented using a digitally controlled optical delay line.

The LaF_3:Pr^{3+} (0.5%) sample is attached to a cold finger which is cooled to 9 K by a two stage closed-cycle refrigerator. The fluorescence from the $^3P_0 \rightarrow {}^3H_6$ transition is collected at 90° to the sample, filtered with a RG600 Schott filter, detected by an Oriel 77341 photomultiplier tube (PMT), and data acquired with a Stanford Research SR400 single gate photon counter.

Using the above experimental setup, the occupation numbers of phonons at frequencies 113, 75, and 55 cm^{-1} are measured as a function of the delay between the FIR and optical pulses. Assuming hyperbolic secant squared pulse profiles for both the 350 ps FIR and the 236 ps optical pulse widths, respectively, the phonon lifetimes are deconvoluted from the measured transients as detailed below.

III. RESULTS AND DISCUSSION

Figure 3 shows phonon transients at frequencies: (a) 113 cm^{-1}, (b) 75 cm^{-1}, and (c) 55 cm^{-1}. We note that the light solid line in these traces merely serves as a guide to the eye.

Two features are immediately apparent from Fig. 3: (i) The phonon decay rate increases rapidly with frequency. (ii) The peak of each successive transient occurs at progressively later times. The latter feature is consistent with the lower frequency phonons being decay products of the initial 113 cm^{-1} phonon population.

The phonon lifetimes are deconvoluted from the transients in Fig. 3 by first assuming a hyperbolic secant squared form for the FIR pump pulse, $P_{\mathrm{FIR}}(t)$, with a pulsewidth of 350 ps. The following rate equations are then solved for $N_1(t)$, the occupation number of the 113 cm^{-1} phonons, coupled to $N_i(t)$, the occupation number of the ith phonon population

$$\frac{dN_1(t)}{dt} = P_{\mathrm{FIR}}(t) - \sum_i R_{1i} N_1(t), \tag{1}$$

$$\frac{dN_i(t)}{dt} = R_{1i} N_1(t) - \sum_j R_{ij} N_i(t), \tag{2}$$

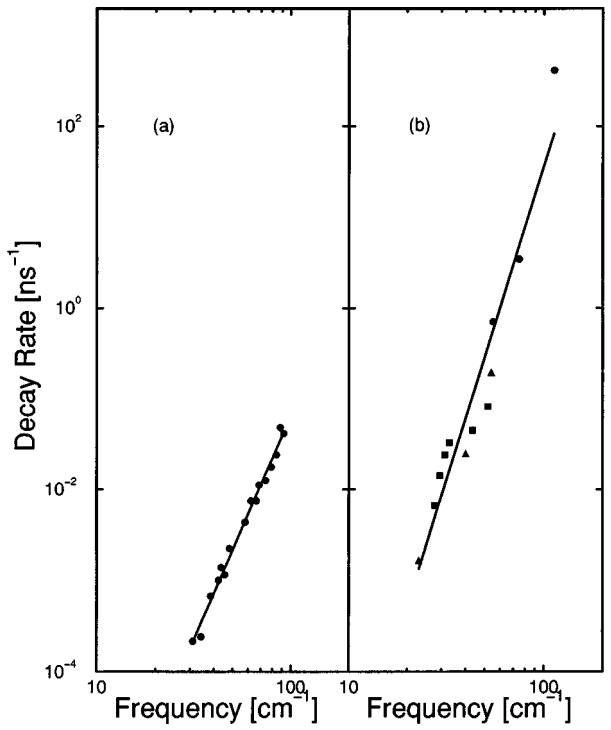

FIG. 4. Anharmonic decay rate versus phonon frequency for: (a) $LiYF_4:Pr^{3+}$ and (b) $LaF_3:Pr^{3+}$. The solid lines are power-law fits to the data with exponents 4.9 ± 0.1 and 6.6 ± 0.6, respectively.

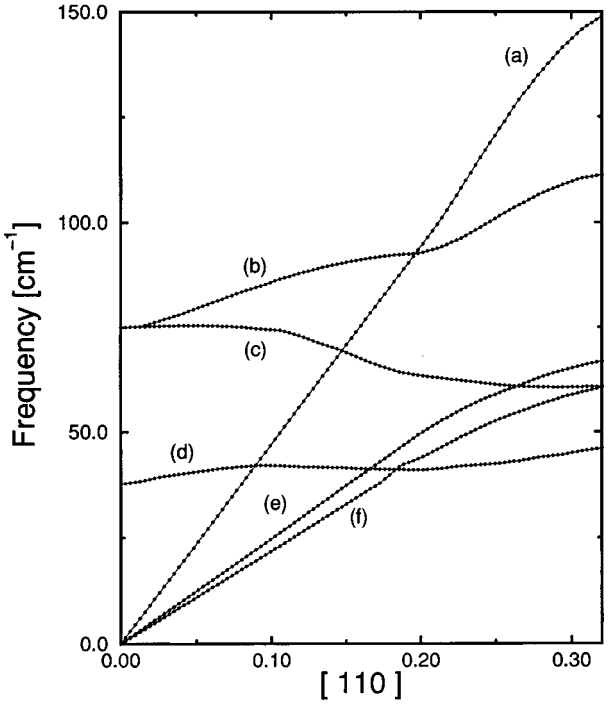

FIG. 5. Dispersion curves for LaF_3 in the (110) direction. These curves are an interpolation of experimental data (see text). Key: (a) LA, (b) LO, (c) $TO_{\parallel}$, (d) $TO_{\parallel,\perp}$, (e) $TA_{\perp}$, (f) $TA_{\parallel}$. Note the low-lying optical modes that intersect the acoustic branches.

where R_{ij} is the relaxation rate of a phonon population i into a lower frequency phonon population j. The functions $N_i(t)$ are then convoluted with the optical probe pulse, $P_{\mathrm{OPT}}(t)$, a squared hyperbolic secant with pulsewidth 236 ps, in order to calculate $M_i(\tau)$ which can be compared with the experimental data. Where

$$M_i(\tau)=\int_{-\infty}^{\infty} N_i(t)P_{\mathrm{OPT}}(\tau-t)dt. \tag{3}$$

The best fit to the measured data is found by varying the set of decay rates R_{ij} and performing a least-squares fit of $M_i(\tau)$ to the data. Using this method of deconvolution, we obtain values for the decay times of the phonons of 2.5 ± 1 ps at $113\,\mathrm{cm}^{-1}$, 293 ± 17 ps at $75\,\mathrm{cm}^{-1}$, and 1.4 ± 0.15 ns at $55\,\mathrm{cm}^{-1}$. The heavy solid lines in Fig. 3 are the resulting fits to the data.

An isotropic model with linear dispersion predicts that nonequilibrium phonons near the zone center will have an anharmonic decay rate proportional to ω^5, where ω is the frequency of the phonon population. A typical example of this behavior is shown in Fig. 4(a) for $LiYF_4:Pr^{3+}$.[14] A power-law fit to this data yields an exponent of 4.9 ± 0.1, in good agreement with the predicted ω^5 dependence. Tolbert, Dennis, and Yen,[1] and Meltzer, Rives, and Dixon,[2] have measured the anharmonic decay rates of phonons in the frequency range of $22-54\,\mathrm{cm}^{-1}$. These data (squares and triangles, respectively) are shown in Fig. 4(b). Adding our results (circles) to Fig. 4(b), we find that a power-law fit gives an exponent of 6.6 ± 0.6, indicating a significant deviation from the isotropic model with linear dispersion.

Figure 5 shows the dispersion curves for LaF_3 in the [110] direction revealing[15] low-lying optical modes that intersect the acoustic branches. This is in contrast to most materials in which the optical modes lie at higher frequencies than the acoustic modes. It is usual for a longitudinal-acoustic phonon to decay either into two transverse-acoustic phonons or into one transverse-acoustic and one longitudinal-acoustic phonon. Taking into account the presence of these low-lying optical modes, additional decay processes for longitudinal-acoustic phonons become possible, i.e., a longitudinal-acoustic phonon can decay into one transverse-optical phonon and one transverse-acoustic phonon. It is expected that these additional decay processes will contribute to the total relaxation rate of the higher frequency phonons and cause a deviation from the expected ω^5 dependence.

In order to detail the effects of these low-lying optical modes, a calculation of the phonon anharmonic decay rate is performed for an isotropic system based on the experimentally derived dispersion curves of Fig. 5.[15] The results presented are based on the [110] direction of this system, as this is the direction of lowest symmetry for which dispersion data exists. It should be noted that the transverse-acoustic phonons (TA), which are degenerate in higher symmetry directions, split into $TA_{\perp}$ and $TA_{\parallel}$ branches in this direction. In addition, calculations based on dispersion curves from either the [100] or the [001] directions yield qualitatively similar results.

The single mode relaxation time, $\tau_{\mathbf{q}s}$, for the anharmonic three phonon process, at low temperature is given by[16]

$$\tau_{\mathbf{q}s}^{-1}\propto\sum_{\mathbf{q}'s'\mathbf{q}''s''}|A^{ss's''}_{\mathbf{q}\mathbf{q}'\mathbf{q}''}|^2\,\frac{qq'q''}{c_s c_{s'} c_{s''}}\times\delta_{\mathbf{q}+\mathbf{q}'+\mathbf{q}''}\cdot\delta(\omega(\mathbf{q}s)-\omega(\mathbf{q}'s')-\omega(\mathbf{q}''s'')), \tag{4}$$

where the $A^{ss's''}_{\mathbf{qq'q''}}$ are the Fourier components of the phonon coupling constants, $\mathbf{q}$, $\mathbf{q}'$, and $\mathbf{q}''$ are the wave vectors of a parent phonon and daughter phonons, respectively. The velocity of the branch with polarization s is given by c_s, while ω denotes the frequency. Note that in the absence of additional information the $A^{ss's''}_{\mathbf{qq'q''}}$ are taken to be the same for all decay processes.[16]

The numerical evaluation of $\tau_{\mathbf{q}s}$, proceeds as follows. The energy and wave vector of a parent phonon is selected from the dispersion curves. The wave vector of the first daughter phonon is then selected from a cubic mesh of 106 points in an octant of the Brillouin zone and the energy again determined from the dispersion curves. Energy and wave-vector conservation determines the second daughter phonon. The total phonon decay rate is then obtained by summing over all processes. The complexity of the dispersion curves results in 53 possible anharmonic decay processes. Figure 6 illustrates the five dominant decay processes.

An examination of Fig. 6 shows that the frequency dependence of the phonon relaxation rate for the processes $LA \rightarrow TA_\perp + TA_\perp$ and $LA \rightarrow TA_\perp + TA_\parallel$ is in good agreement with the isotropic dispersionless model as expected. Of particular note in Fig. 6 is the $LA \rightarrow TA_\parallel + TO_{\parallel,\perp}$ decay process. This process exhibits a frequency dependence of the anharmonic decay rate that is significantly steeper than ω^5. The three-phonon anharmonic relaxation of LA phonons at high frequencies may become dominated by this decay path. Finally we point out that the transverse-optical phonons with frequencies around 40 and 70 cm^{-1} may be extremely long lived.

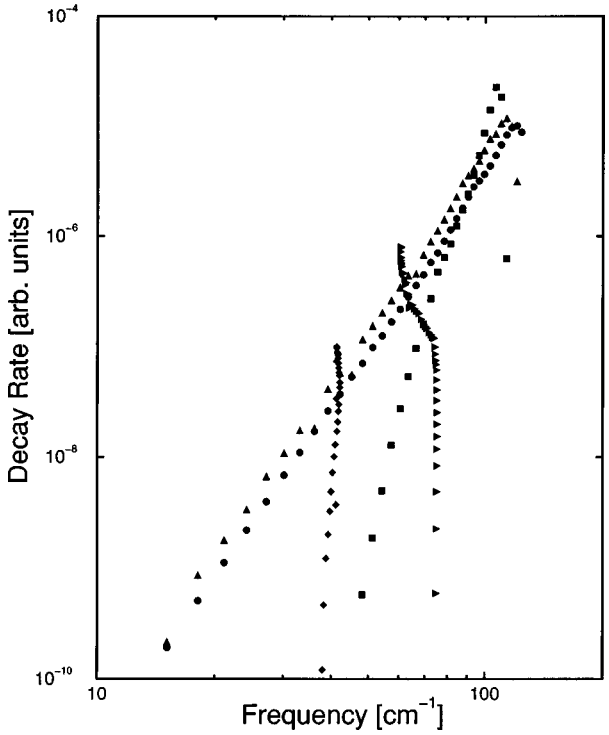

FIG. 6. The five dominant decay processes calculated from the dispersion curves of Fig. 5 and Eq. (4). Key: ■: $LA \rightarrow TA_\parallel + TO_{\parallel,\perp}$; ▲: $LA \rightarrow TA_\perp + TA_\perp$; ●: $LA \rightarrow TA_\perp + TA_\parallel$; ▶: $TO_\parallel \rightarrow TA_\parallel + TO_{\parallel,\perp}$; ◆: $TO_{\parallel,\perp} \rightarrow TA_\perp + TA_\parallel$.

IV. CONCLUSIONS

We have generated subnanosecond FIR pulses using a semiconductor plasma switching technique. We have shown that these pulses can be used to increase the temporal resolution of phonon spectroscopy measurements using defect-induced one-phonon absorption for phonon generation in $LaF_3:Pr^{3+}$. We have measured a deviation from the ω^5 dependence of the phonon decay rate predicted by the usual isotropic model with linear dispersion. A possible source of this deviation may be due to the detailed form of the dispersion curves.

Using a more realistic model for the dispersion curves in this system, we have calculated the decay rates for individual relaxation processes. We have found that the presence of low-lying optic modes can indeed cause the decay rate of the acoustic modes to exhibit a frequency dependence which is steeper than ω^5. Finally, we note that low-lying optic modes may exhibit extremely slow relaxation rates.

ACKNOWLEDGMENTS

This work was supported by the National Science Foundation, Grant No. DMR-93-21052. The authors would like to thank D. L. Huber and P. G. Klemens for useful discussions. S. M. K. would like to thank the University of Georgia Graduate School for additional support.

*Present address: Code 5640, Laser Physics Branch, U.S. Naval Research Laboratory, Washington, D.C. 20375.

[1] W. A. Tolbert, W. M. Dennis, and W. M. Yen, Phys. Rev. B **44**, 2149 (1991).

[2] R. S. Meltzer, J. E. Rives, and G. S. Dixon, Phys. Rev. B **28**, 4786 (1983).

[3] R. Orbach and L. A. Vredevoe, Physics (Long Island City, N.Y.) **1**, 91 (1964).

[4] P. G. Klemens, J. Appl. Phys. **38**, 4573 (1967).

[5] W. A. Tolbert, W. M. Dennis, and W. M. Yen, Phys. Rev. Lett. **65**, 607 (1990).

[6] A. J. Alcock, P. B. Corkum, and D. J. James, Appl. Phys. Lett. **27**, 680 (1975).

[7] Claude Rolland and P. B. Corkum, J. Opt. Soc. Am. B **3**, 1625 (1986).

[8] H. Salzmann, T. Vogel, and G. Dodel, Opt. Commun. **47**, 340 (1983).

[9] See, for example, Jacques I. Pankove, *Optical Processes in Semiconductors* (Dover, New York, 1975), Chaps. 3 and 18.

[10] Cornelius T. Gross, Joachim Kiess, Arnold Mayer, and Fritz Keilmann, IEEE J. Quantum Electron. **QE-23**, 377 (1987).

[11] See, for example, C. Kittel, *Introduction to Solid State Physics* (Wiley, New York, 1986).

[12] Michael Shur, *Physics of Semiconductors Devices* (Prentice Hall, Englewood Cliffs, NJ, 1990), Chap. 1.

[13] M. S. Tyagi and R. Van Overstraaten, Solid-State Electron. **26**, 577 (1983).
[14] Xiao-jun Wang, W. M. Dennis, and W. M. Yen, Phys. Rev. B **46**, 8168 (1992).
[15] G. Dixon and R. M. Nicklow, Solid State Commun. **47**, 2149 (1984).
[16] G. P. Srivastava, *The Physics of Phonons* (Hilger, Bristol, 1990).